



HAL
open science

Directionally induced quasi-phase matching in homogeneous AlGaAs waveguides

N. Morais, I. Roland, M. Ravaro, W. Hease, A. Lemaître, C. Gomez, S. Wabnitz, M. de Rosa, I. Favero, G. Leo

► **To cite this version:**

N. Morais, I. Roland, M. Ravaro, W. Hease, A. Lemaître, et al.. Directionally induced quasi-phase matching in homogeneous AlGaAs waveguides. *Optics Letters*, 2017, 42 (21), pp.4287. 10.1364/OL.42.004287. hal-04224681

HAL Id: hal-04224681

<https://hal.science/hal-04224681>

Submitted on 2 Oct 2023

HAL is a multi-disciplinary open access archive for the deposit and dissemination of scientific research documents, whether they are published or not. The documents may come from teaching and research institutions in France or abroad, or from public or private research centers.

L'archive ouverte pluridisciplinaire **HAL**, est destinée au dépôt et à la diffusion de documents scientifiques de niveau recherche, publiés ou non, émanant des établissements d'enseignement et de recherche français ou étrangers, des laboratoires publics ou privés.

Directionally induced quasi-phase matching in homogeneous AlGaAs waveguides

N. MORAIS¹, I. ROLAND¹, M. RAVARO¹, W. HEASE¹, A. LEMAÎTRE², C. GOMEZ², S. WABNITZ^{3,4}, M. DE ROSA⁴, I. FAVERO¹, AND G. LEO^{1,*}

¹ *Matériaux et Phénomènes Quantiques, Université Paris Diderot, CNRS, Sorbonne Paris Cité, 10 rue Domon et Duquet, 75013 Paris, France*

² *Centre de Nanosciences et de Nanotechnologies, CNRS, Univ. Paris-Sud, Université Paris-Saclay 91460 Marcoussis, France*

³ *Department of Information Engineering, University of Brescia, Via Branze 38, 25123 Brescia, Italy*

⁴ *CNR-INO, Istituto Nazionale di Ottica, Via Campi Flegrei 34, 80078 Pozzuoli, Italy*

*Corresponding author: giuseppe.leo@univ-paris-diderot.fr

Received XX Month XXXX; revised XX Month, XXXX; accepted XX Month XXXX; posted XX Month XXXX (Doc. ID XXXXX); published XX Month XXXX

We report on the experimental observation of quasi-phase matching (QPM) in a homogeneous waveguide. By fabricating a monolithic snake-shaped suspended AlGaAs nanowire on a (001) GaAs wafer, we demonstrate the unraveled version of a $\chi^{(2)}$ whispering-gallery mode microdisk, obtaining second harmonic generation (SHG) in the optical telecom wavelength range. With a radius of curvature of 50 μm and four spatial oscillations along the (110) average direction, a splitting of the second-harmonic spectrum occurs around the phase-matching wavelength of the corresponding straight waveguide. This splitting, which increases as the radius of curvature decreases, provides a useful degree of freedom for the design of small-footprint nonlinear photonic devices on-chip.

OCIS codes: (130.3120) *Integrated optics devices*; (160.4330) *Nonlinear optical materials*; (160.6000) *Semiconductor materials*; (190.4360) *Nonlinear optics, devices*.

<http://dx.doi.org/10.1364/OL.99.099999>

Total internal reflection in propagation-invariant, transversely confining dielectric structures is commonly exploited for non-diffracting high-intensity propagation of light, providing an ideal environment for nonlinear physics and engineering. If we focus on guided-wave $\chi^{(2)}$ effects in the near infrared, most waveguides are made of birefringent ferroelectrics such as lithium niobate and KTP. Such waveguides provide weak photon confinement owing to their relatively low refractive index contrast between the core and the cladding. Although their correspondingly large cross sections (up to 10 μm^2) have not hindered the demonstration of a large number of nonlinear interactions, including classical and quantum effects [1,2], weak confinement results in relatively bulky structures that are hardly integratable with laser diodes and photodiodes. In order to reduce the footprint of nonlinear photonic devices and open the way to their optoelectronic integration, today

a viable option is provided by the use of high-refractive-index-contrast semiconductor waveguides.

Several types of high-contrast nonlinear integrated structures have been demonstrated in the last years, spanning from nanowires [3,4] to high- Q resonators [5-7] and multi-pole nanoantennas [8]. To confine photons at sub-wavelength scales, such devices rely on a high-refractive-index core clad by a far lower index in two or three dimensions, and therefore they typically consist of semiconductor nanostructures that either lie on an oxide substrate or are suspended in air. A promising semiconductor for monolithic photonics is aluminum gallium arsenide (AlGaAs) [9-11]. Besides having a high optical Kerr coefficient, this III-V alloy has a high $\chi^{(2)}$; it is a mature laser material; and its direct band-gap can be varied with the Al molar fraction, making it not only linearly transparent from 0.7 μm to 16 μm , but also two-photon-absorption free at 1.55 μm . The AlGaAs cubic structure and its non-ferroelectric nature have spurred a number of methods for ensuring phase matching, as reviewed in Ref. [12]. More recently, SHG based on modal phase matching in a wafer-bonded structure [4] and optical parametric oscillation (OPO) based on form birefringence [13] have also been demonstrated in partially oxidized AlGaAs waveguides. Conversely, guided-wave QPM in the near infrared is still challenging, due to high optical losses associated with epitaxial regrowth over a staggered micro-structured substrate [14].

To avoid the technological burden of QPM crystal orientation, one can resort to zig-zag phase-matching, where the nonlinear polarization along the propagation direction is periodically phased matched by a combination of linear (Fresnel reflection) and nonlinear (change of sign of the effective $\chi^{(2)}$) effects. Such concept dates back to Bloembergen's seminal paper [15], and was developed by Haïdar et al. [16]. More recently, an effective QPM in $\bar{4}$ symmetry ($\bar{4}$ QPM) was recognized to occur in zinc-blend homogeneous whispering-gallery-mode cavities [17], and proven experimentally for GaAs [5] and AlGaAs [6] microdisks.

Here we report the design, fabrication and characterization of a periodically bent, "snake" AlGaAs suspended nanowire with sub-

wavelength cross section. In this new type of waveguide, we achieve SHG with a pump in the telecom wavelength range in what can be seen as the unraveled version of the SHG in a suspended microdisk [18]. Since phase matching between the $TE_{00}(\omega)$ and $TM_{00}(2\omega)$ modes of a homogeneous AlGaAs nanowire typically occurs for small transverse sections with strongly asymmetric aspect ratios [19], we are motivated to demonstrate a novel degree of freedom in order to phase-match SHG (or other $\chi^{(2)}$ processes) in small footprint devices on-chip.

To better illustrate the essence of our proof-of-principle, let us start from a straight $Al_{0.19}Ga_{0.81}As$ nanowire in air. Using a homemade finite-difference code and a commercial finite-element package based on Gehrsitz dispersion model [20], we predict type-1 birefringent phase matching between a TE_{00} mode at ω (at a wavelength $\lambda_\omega = 1.57 \mu m$) and a TM_{00} mode at 2ω (at $\lambda_{2\omega} = \lambda_\omega/2$), for a rectangular cross section with height $h = 123 \text{ nm}$ and width $w = 1 \mu m$. Then, our aim being to explore the effect of an additional $\bar{4}$ QPM, we perturb such phase-matched SHG with a four-period snake-shaped bending. Figure 1 illustrates the $\bar{4}$ QPM principle in the case of interest here, where the snake waveguide is oriented along the $\langle 110 \rangle$ direction, *i.e.*, with the end-fire facets parallel to GaAs cleavage planes. The effective nonlinearity is $d_{\text{eff}} = (1/2)d_{14}\sin 2\varphi$, with φ the angle between the propagation direction and the crystallographic axis $\langle 100 \rangle$ [18]. Its profile along the nanowire curvilinear abscissa s is shown in Fig. 1d, with a radius of curvature $R = 50 \mu m$, a nonlinear period $A = 2L_c = \pi R$, and $d_{14} = 119 \text{ pm/V}$ [21,22].

Fabrication follows the guidelines of Figure 2. We begin with a planar structure consisting of a 123 nm film of $Al_{0.19}Ga_{0.81}As$ on a 4 μm $Al_{0.8}Ga_{0.2}As$ sacrificial layer, grown on a GaAs {001} substrate by molecular beam epitaxy. Electron-beam lithography is used to define the pattern of the nanowires and their anchoring points, followed by Ar/SiCl₄-assisted inductively coupled plasma reactive ion etching. Then we define a mesa by optical lithography, which we etch chemically with a solution of 1/3 of acetic acid, 1/3 of bromic acid and 1/3 of saturated solution of $K_2Cr_2O_7$ in deionized water. This mesa is crucial for the optical measurements. Under-etching of the sacrificial layer is made by a 1% HF solution at 4°C, and the sample undergoes critical-point drying. The result is a monolithic structure with snake-shaped nanowires consisting of cascaded half-circles with opposite curvatures and overall length

of about 1.46 mm, including two straight inverted tapers for end-fire coupling. Two scanning-electron-microscope (SEM) pictures of the waveguide are shown in Fig. 3, where the anchoring points are visible as well as the inverted tapers for impedance-matched input and output coupling using micro-lensed fibers.

The first characterization step deals with the linear optical losses of the interacting modes at ω and 2ω . In these nanowires, losses arise from different sources: 1) radiation at the bent interface between the waveguide and the air; 2) mode-overlap mismatch at every inversion of the curvature; 3) surface states due to fabrication imperfections, especially roughness of the etched side walls; and 4) non-ideal end-fire power coupling into and out of the inverted tapers. Two continuous-wave sources are used: an external-cavity laser diode at wavelengths ranging from 1500 to 1620 nm (ω), and a Ti:Sapphire laser emitting at 700-1000 nm (2ω). Light is detected by InGaAs and Si photodiodes at ω and 2ω , respectively, and input/output coupled via micro-lensed fibers. We begin with estimating the loss coefficient α_1 of a straight nanowire of length $L_1 = 200 \mu m$ on a dummy taper-less sample, via Fabry-Perot fringes, finding $\alpha_1 = 3.7 \pm 0.4 \text{ cm}^{-1}$ at ω (TE) and $\alpha_1 = 38 \pm 12 \text{ cm}^{-1}$ at 2ω (TM). Higher losses at 2ω are compatible with sidewall defects [6]. Moreover our waveguides, which are vertically single mode at ω and 2ω , are laterally multimode at both frequencies, resulting in an overestimation of α_1 , especially at 2ω [23]. Excluding injection and collection losses, the power fraction transmitted along the straight waveguide is $T_1 = \exp(-\alpha_1 L_1)$. Next, we determine the coupling losses between the inverted tapers and the micro-lensed fibers. For that, we measure the total transmission of a straight waveguide of the same length L_1 , to which we added two inverted tapers at the ends. The latter is $T_2 = T_c^2 T_1$, with T_c the light fraction that is coupled between the micro-lensed fiber and the inverted taper. The measured values of T_c are $61.4 \pm 0.2\%$ at ω and $10 \pm 1\%$ at 2ω , which compare fairly well with the maximum coupling efficiencies of 80% (at ω) and 45% (at 2ω) calculated by 3D FDTD. Notice that the measured T_c is under-estimated due to the overestimation of α_1 . Finally, we measure the total transmission T_3 of the snake-shaped nanowire of length $L_3 = 8\pi R \approx 1.26 \text{ mm}$, where $T_c^2 T_1 T_{\text{snake}} = T_2 T_{\text{snake}} = T_3$, with T_1 the contribution of the straight segments at the ends of the nanowire, of length $L_1/2$ each. We find a loss coefficient $\alpha_{\text{snake}} = -(1/L_3)\ln(T_{\text{snake}}) = 4.5 \pm 0.1 \text{ cm}^{-1}$ at ω and $\alpha_{\text{snake}} = 64 \pm 4 \text{ cm}^{-1}$ at 2ω .

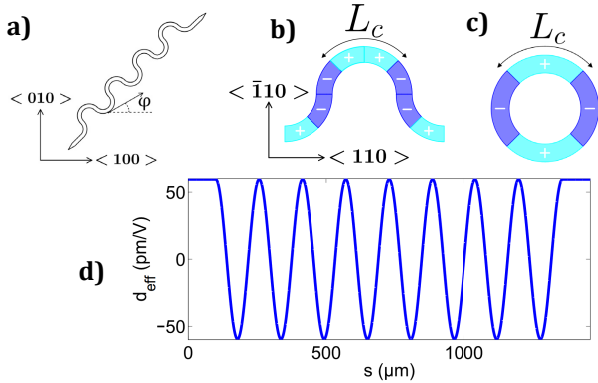


Fig. 1. Principle: a) layout and orientation of a 4-period snake nanowire; b) sequence of $\pi/4$ arcs within one period, with a coherence length L_c equal to a $\pi/2$ arc; c) ring with the same orientation as the waveguide; d) d_{eff} along the waveguide.

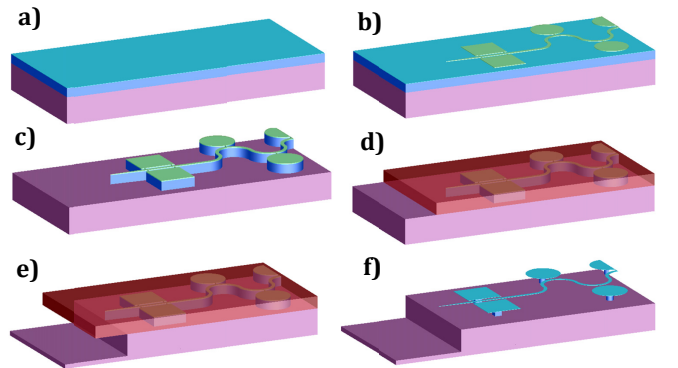


Fig. 2. Fabrication: a) clean wafer; b) e-beam lithography; c) RIE-ICP etching; d) optical lithography to define the mesa; e) BCK etching; f) HF under-etching and critical point drying.

Figure 4a shows the phase mismatch Δk of a straight nanowire with $h = 123$ nm, vs. pump wavelength λ and nanowire width w . Despite the finite precision of this calculation, the $\Delta k = 0$ line at the center of the map shows that phase matching should occur in the straight nanowire within the fabrication tolerances on w and h , and throughout the experimental pump wavelength range. For $\lambda = 1593$ nm, the calculated effective indices of the interacting $TE_{00}(\omega)$ and $TM_{00}(2\omega)$ modes are traced vs. w in the inset of Fig. 4a, their intersection corresponding to type-1 phase matching.

In order to measure SHG spectra, we injected in both the straight and the snake nanowires 0.8 mW of the same TE-polarized tunable diode beam used for the linear measurements at ω , and we collected the SHG field at 2ω with the Si photodiode connected to a trans-impedance and a lock-in amplifier. No band-pass filter around the second harmonic frequency was necessary, because the Si photodiode is blind in the pump wavelength range.

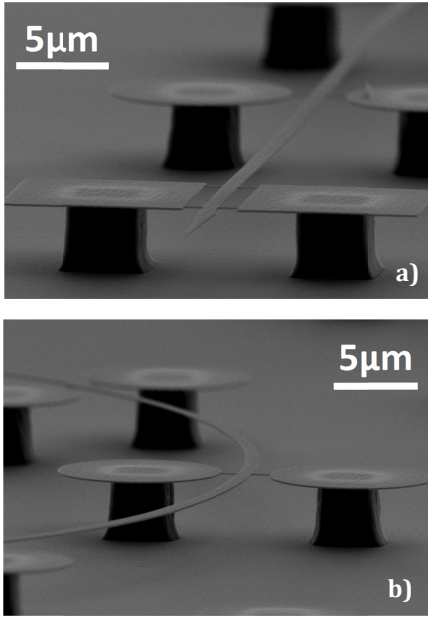


Fig. 3. SEM images of: a) a coupling inverted taper; b) a bend in the snake waveguide.

To appreciate the role of QPM in the snake waveguide, we report in Fig. 4b two SHG efficiency spectra, obtained by dividing the second-harmonic power spectrum by the square of the pump laser power. The thick black curve shows the SHG efficiency for a straight nanowire of length 1 mm oriented along the $\langle 110 \rangle$ direction. Its central wavelength is best fit by the value $w = 0.82 \pm 0.04$ μm of the waveguide width (marked in Fig. 4a by a vertical dashed line) that fulfills the phase-matching condition, $\Delta k = k_{2\omega} - 2k_{\omega} = 0$. This width is smaller than the nominal 1 μm width of our resist mask, whose borders are slightly etched during the dry-etching, but is compatible with the non-uniform width of the fabricated waveguide, observed by SEM (0.90 ± 0.05 μm). The thick red curve shows the SHG efficiency spectrum of a snake-shaped nanowire with the same cross section and average orientation, and length ≈ 1.46 mm. It systematically reveals two distinct QPM spectral features around the wavelengths $\lambda_1 = 1591$ nm and $\lambda_2 = 1596$ nm, which are in excellent agreement with the calculated

QPM condition $\Delta k = k_{2\omega} - 2k_{\omega} = \pm 2\pi/\Lambda = \pm 2/R$. These two wavelengths are reported in Fig. 4a as white dots. The measured peak SHG efficiency is 1.2% W^{-1} for the snake nanowire and 2.7% W^{-1} for the straight nanowire, respectively. Using the same best-fit value of w , we also plotted in Fig. 4b the calculated lossless phase-matching curves of both the snake-shaped (red thin line) and the straight nanowire (black thin line). As suggested by side-lobes visibility, the different spectral widths of the theoretical and experimental curves can only in part be due to propagation losses, and they are tentatively attributed to inhomogeneous waveguide width along its length. It is straightforward to derive the relation between the two QPM wavelengths λ_1 and λ_2 in the SHG spectrum of a snake-shaped nanowire:

$$\frac{n_{\lambda_1/2} - n_{\lambda_1}}{\lambda_1} - \frac{n_{\lambda_2/2} - n_{\lambda_2}}{\lambda_2} = \frac{1}{\pi R}, \quad (1)$$

where n_{λ} is the effective index at wavelength λ . Equation 1 says that the distance between the two peaks in the SHG spectrum of a snake-shaped nanowire depends inversely on the curvature radius of its bends. Increasing the peak spectral separation by reducing the radius requires some care to manage the increase of bending losses and overlap mismatch losses. In the case presented here, where the radius of curvature is relatively large, the main source of losses is given by surface states due to fabrication non-idealities, since the calculated overall losses at ω and 2ω are expected to be smaller than 0.6 cm^{-1} , i.e. mode-overlap-mismatch losses at 2ω .

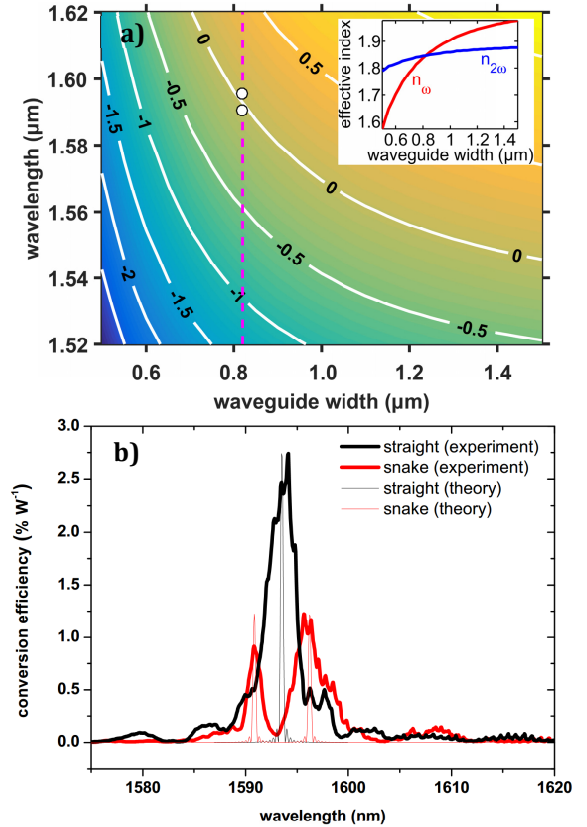


Fig. 4. a) Calculated map of phase mismatch Δk (μm^{-1}) vs. w and λ , for $h = 123$ nm. Inset: effective indices of TE_{00} mode at ω (red line) and TM_{00} mode at 2ω (blue line) vs. w , for $\lambda = 1593$ nm. b) Experimental (thick line) and calculated (thin line) SHG spectra of a straight nanowire (black) and a snake-shaped nanowire (red).

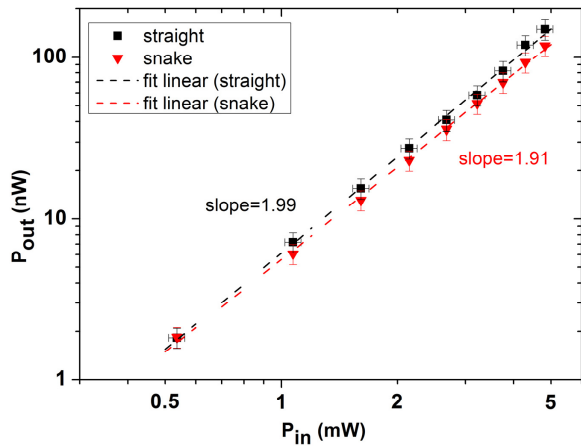


Fig. 5. SHG power at phase matching for a straight (black) and snake-shaped (red) nanowire: experimental data (dots) and linear fits (dashed lines).

One way to decrease mode-overlap-mismatch losses would be to make a smooth transition in the change of curvature, either by using a sinusoidal shaped waveguide [18] or other types of waveguide bends, like in Euler's method of natural equations [24]. In such optimized version of our waveguide, we can estimate $R = 2 \mu\text{m}$ as a realistic lower limit for the radius of curvature (corresponding to $\alpha < 1 \text{ cm}^{-1}$), which sets an upper limit for the spectral splitting to $\lambda_2 - \lambda_1 \approx 145 \text{ nm}$.

Finally, Fig. 5 shows the log-log plot of the SHG power at phase matching, versus the injected power at the fundamental frequency for both waveguides. The experimental points follow straight lines of slope ≈ 2 , as it is expected from the quadratic dependence of SHG power on injected power.

In conclusion, we have demonstrated quasi-phase-matched SHG in a snake-shaped suspended AlGaAs nanowire, and we have observed for the first time the splitting of a QPM spectrum in a homogeneous waveguide around the phase-matching wavelength of the associated straight waveguide. Our result is relevant under different perspectives: 1) it provides a useful degree of freedom for phase matching frequency conversion in small footprint devices on-chip (please notice that, regardless the fact that here we reach phase matching also in the straight waveguide for demonstration purposes, future designs might usefully address practical cases where phase matching is out of reach in a straight waveguide); 2) it opens the perspective of exploiting the splitting of the QPM spectrum in quantum photonic devices on-chip, on the guidelines of the recent work of Laudenbach et al. in bulk PPKTP [25]; 3) it is a significant step towards a snake waveguide resonator for efficient generation of coherent optical frequency combs, based on cascaded $\chi^{(2)}$ interactions [26]. The latter is indeed a promising candidate for achieving a comb generation threshold in the microwatt range, in a highly competitive context where sub-milliwatt OPO threshold has been very recently achieved in $\chi^{(3)}$ silicon nitride microrings [27]. While optimization issues are clearly outside of the scope of this proof-of-principle Letter, we are currently fabricating a more performing version of the $\chi^{(2)}$ snake nanowire, based on the AlGaAs-on-AlOx platform.

Funding. G. Leo and S. Wabnitz acknowledge CNR and Paris Diderot University for supporting two visiting periods as invited professors in both institutions. I. Roland post-doc was funded by SATT IdF-Innov. M. De Rosa acknowledges support from CNR

(Short Term Mobility Program 2016). M. De Rosa and S. Wabnitz are supported by Ministero dell'Istruzione, dell'Università e della Ricerca (Project PRIN-2015KEZNYM).

Acknowledgment. The authors warmly thank A. De Rossi for fruitful discussions.

References

1. T. Suhara and M. Fujimura, "Waveguide Nonlinear-Optic Devices", Springer (2003).
2. O. Alibart, V. D'Auria, M. De Micheli, F. Doutré, F. Kaiser, L. Labonté, T. Lunghi, E. Picholle, S. Tanzilli, *IOP J. of Optics*, **18**, 104001 (2016).
3. L. Scaccabarozzi, M. Fejer, Y. Huo, S. Fan, X. Yu, and J. Harris, *Opt. Lett.* **31**, 3626-3629 (2006).
4. T. Matsushita, Y. Nakamura, S. Matsumoto, T. Onda, I. Shoji, and T. Kondo, *Conference on Lasers and Electro-Optics - Pacific Rim*, (Optical Society of America, 2013), pap. WA3-3.
5. P. S. Kuo, J. Bravo-Abad, and G. S. Solomon, *Nat. Commun.* **5**, 3109 (2014).
6. S. Mariani, A. Andronico, A. Lemaître, I. Favero, S. Ducci, and G. Leo, *Opt. Lett.* **39**, 3062-3065 (2014).
7. M. Pu, L. Ottaviano, E. Semenova, and K. Yvind, *Optica* **3**, 823-826 (2016).
8. V. F. Gili, L. Carletti, A. Locatelli, D. Rocco, M. Finazzi, L. Ghirardini, I. Favero, C. Gomez, A. Lemaître, M. Celebrano, C. De Angelis, and G. Leo, *Opt. Express* **24**, 15965-15971 (2016).
9. J. Wang, A. Santamato, P. Jiang, D. Bonneau, E. Engin, J. W. Silverstone, M. Lerner, J. Beetz, M. Kamp, S. Höfling, M. G. Tanner, C. M. Natarajan, R. H. Hadfield, S. N. Dorenbos, V. Zwiller, J. L. O'Brien, M. G. Thompson, *Opt. Comm.* **49**, 327 (2014).
10. D. Kang, A. Pang, Y. Zhao, A. Helmy, *J. Opt. Soc. Am. B* **31**, 1581 (2014).
11. P. Apiratikul, J. Wathen, G. Porkolab, B. Wang, L. He, T. Murphy, and C. Richardson, *Opt. Express* **22**, 26814, (2014).
12. A. S. Helmy, P. Abolghasem, J. S. Aitchison, B. J. Bijlani, J. Han, B. M. Holmes, D. C. Hutchings, U. Younis, and S. J. Wagner, *Laser & Photon. Rev.* **5**, 272-286 (2011).
13. M. Savanier, C. Ozanam, L. Lanco, X. Lafosse, A. Andronico, I. Favero, S. Ducci, and G. Leo, *Appl. Phys. Lett.* **103**, 261105 (2013).
14. X. Yu, L. Scaccabarozzi, J. S. Harris, P. S. Kuo, and M. M. Fejer, *Opt. Express* **13**, 10742-10748 (2005).
15. J. A. Armstrong, N. Bloembergen, J. Ducuing, and P. S. Pershan, *Phys. Rev.* **127**, 1918-1939 (1962).
16. R. Haïdar, N. Forget, P. Kupecek, and E. Rosencher, *J. Opt. Soc. Am. B* **21**, 1522-1534 (2004).
17. Y. Dumeige and P. Feron, *Phys. Rev. A* **74**, 063804 (2006).
18. R. T. Horn and G. Weihs, arXiv:1008.2190 (2010).
19. H. Ishikawa and T. Kondo, *Appl. Phys. Express* **2**, 042202 (2009).
20. S. Gehrsitz, F. K. Reinhart, C. Gourgon, N. Herres, A. Vonlanthen, and H. Sigg, *J. Appl. Phys.* **87**, 7825 (2000).
21. I. Shoji, T. Kondo, A. Kitamoto, M. Shirane, and R. Ito, *J. Opt. Soc. Am. B* **14**, 2268-2294 (1997).
22. M. Ohashi, T. Kondo, R. Ito, S. Fukatsu, Y. Shiraki, K. Kumata, and S. S. Kano, *J. Appl. Phys.* **74**, 596-601 (1993).
23. A. De Rossi, V. Ortiz, M. Calligaro, L. Lanco, S. Ducci, V. Berger, and I. Sagnes, "Measuring propagation loss in a multimode semiconductor waveguide," *J. Appl. Physics* **97**, 073105 (2005).
24. R. N. Sheehan, S. Horne, and F. H. Peters, *Opt. Quantum Electron.* **40**, 1211-1218 (2008).
25. F. Laudenbach, S. Kalista, M. Hentschel, P. Walther, and H. Hübel, arXiv:1612.06579 (2016).
26. M. Parisi, I. Ricciardi, S. Mosca, N. Morais, T. Hansson, S. Wabnitz, G. Leo, and M. De Rosa, *J. Opt. Soc. Am. B* **34**, 1842-1847 (2017).
27. X. Ji, F. A. S. Barbosa, S. P. Roberts, A. Dutt, J. Cardenas, Y. Okawachi, A. Bryant, A. L. Gaeta, and M. Lipson, *Optica* **4**, 619-624 (2017).

References (with titles)

1. T. Suhara and M. Fujimura, "Waveguide Nonlinear-Optic Devices", Springer (2003).
2. O. Alibart, V. D'Auria, M. De Micheli, F. Doutre, F. Kaiser, L. Labonté, T. Lunghi, E. Picholle, S. Tanzilli, "Quantum photonics at telecom wavelengths based on lithium niobate waveguides," *IOP J. of Optics*, **18**, 104001 (2016).
3. L. Scaccabarozzi, M. Fejer, Y. Huo, S. Fan, X. Yu, and J. Harris, "Enhanced second-harmonic generation in AlGaAs/AlxOy tightly confining waveguides and resonant cavities," *Opt. Lett.* **31**, 3626-3629 (2006).
4. T. Matsushita, Y. Nakamura, S. Matsumoto, T. Onda, I. Shoji, and T. Kondo, "Fabrication of AlGaAs/Alox Waveguides with Inversion-Stacked Core Structure for Higher-Order Modal-Phase Matching Devices" in *Conference on Lasers and Electro-Optics - Pacific Rim*, (Optical Society of America, 2013), pap. WA3-3.
5. P. S. Kuo, J. Bravo-Abad, and G. S. Solomon, "Second-harmonic generation using 4-quasi-phasematching in a GaAs whispering-gallery-mode microcavity," *Nat. Commun.* **5**, 3109 (2014).
6. S. Mariani, A. Andronico, A. Lemaître, I. Favero, S. Ducci, and G. Leo, "Second-harmonic generation in AlGaAs microdisks in the telecom range," *Opt. Lett.* **39**, 3062-3065 (2014).
7. M. Pu, L. Ottaviano, E. Semenova, and K. Yvind, "Efficient frequency comb generation in AlGaAs-on-insulator," *Optica* **3**, 823-826 (2016).
8. V. F. Gili, L. Carletti, A. Locatelli, D. Rocco, M. Finazzi, L. Ghirardini, I. Favero, C. Gomez, A. Lemaître, M. Celebrano, C. De Angelis, and G. Leo, *Opt. Express* **24**, 15965-15971 (2016).
9. J. Wang, A. Santamato, P. Jiang, D. Bonneau, E. Engin, J. W. Silverstone, M. Lermer, J. Beetz, M. Kamp, S. Höfling, M. G. Tanner, C. M. Natarajan, R. H. Hadfield, S. N. Dorenbos, V. Zwiller, J. L. O'Brien, M. G. Thompson, "Gallium arsenide (gaas) quantum photonic waveguide circuits," *Opt. Comm.* **49**, 327 (2014).
10. D. Kang, A. Pang, Y. Zhao, A. Helmy, "Two-photon quantum state engineering in nonlinear photonic nanowires," *J. Opt. Soc. Am. B* **31**, 1581 (2014).
11. P. Apiratikul, J. Wathen, G. Porkolab, B. Wang, L. He, T. Murphy, and C. Richardson, "Enhanced continuous-wave four-wave mixing efficiency in nonlinear AlGaAs waveguides," *Opt. Express* **22**, 26814, (2014).
12. A. S. Helmy, P. Abolghasem, J. S. Aitchison, B. J. Bijlani, J. Han, B. M. Holmes, D. C. Hutchings, U. Younis, and S. J. Wagner, "Recent advances in phase matching of second-order nonlinearities in monolithic semiconductor waveguides," *Laser & Photon. Rev.* **5**, 272-286 (2011).
13. M. Savanier, C. Ozanam, L. Lanco, X. Lafosse, A. Andronico, I. Favero, S. Ducci, and G. Leo, "Near-infrared optical parametric oscillator in a III-V semiconductor waveguide," *Appl. Phys. Lett.* **103**, 261105 (2013).
14. X. Yu, L. Scaccabarozzi, J. S. Harris, P. S. Kuo, and M. M. Fejer, "Efficient continuous wave second harmonic generation pumped at 1.55 μm in quasi-phase-matched AlGaAs waveguides," *Opt. Express* **13**, 10742-10748 (2005).
15. J. A. Armstrong, N. Bloembergen, J. Ducuing, and P. S. Pershan, "Interactions between light waves in a nonlinear dielectric," *Phys. Rev.* **127**, 1918-1939 (1962).
16. R. Härdar, N. Forget, P. Kupecek, and E. Rosencher, "Fresnel phase matching for three-wave mixing in isotropic semiconductors," *J. Opt. Soc. Am. B* **21**, 1522-1534 (2004).
17. Y. Dumeige and P. Feron, "Whispering-gallery-mode analysis of phase-matched doubly resonant second-harmonic generation," *Phys. Rev. A* **74**, 063804 (2006).
18. R. T. Horn and G. Weihs, "Directional quasi-phase matching in curved waveguides," *arXiv:1008.2190* (2010).
19. H. Ishikawa and T. Kondo, "Birefringent Phase Matching in Thin Rectangular High-Index-Contrast Waveguides", *Applied Physics Express* **2**, 042202 (2009).
20. S. Gehrsitz, F. K. Reinhart, C. Gourgon, N. Herres, A. Vonlanthen, and H. Sigg, "The refractive index of Al_xGa_{1-x}As below the band gap: Accurate determination and empirical modeling", *J. Appl. Phys.* **87**, 7825 (2000).
21. I. Shoji, T. Kondo, A. Kitamoto, M. Shirane, and R. Ito, "Absolute scale of second-order nonlinear-optical coefficients," *J. Opt. Soc. Am. B* **14**, 2268-2294 (1997).
22. M. Ohashi, T. Kondo, R. Ito, S. Fukatsu, Y. Shiraki, K. Kumata, and S. S. Kano, "Determination of quadratic nonlinear optical coefficient of Al_xGa_{1-x}As system by the method of reflected second harmonics," *J. Appl. Phys.* **74**, 596-601 (1993).
23. A. De Rossi, V. Ortiz, M. Calligaro, L. Lanco, S. Ducci, V. Berger, and I. Sagnes, "Measuring propagation loss in a multimode semiconductor waveguide," *J. Appl. Physics* **97**, 073105 (2005).
24. R. N. Sheehan, S. Horne, and F. H. Peters, "The design of low-loss curved waveguides," *Opt. Quantum Electron.* **40**, 1211-1218 (2008).
25. F. Laudenbach, S. Kalista, M. Hentschel, P. Walther, and H. Hübner, "A novel single-crystal & single-pass source for polarisation- and colour-entangled photon pairs," *arXiv:1612.06579* (2016).
26. M. Parisi, I. Ricciardi, S. Mosca, N. Morais, T. Hansson, S. Wabnitz, G. Leo, and M. De Rosa, "AlGaAs waveguide microresonators for efficient generation of quadratic frequency combs," *J. Opt. Soc. Am. B* **34**, 1842-1847 (2017).
27. X. Ji, F. A. S. Barbosa, S. P. Roberts, A. Dutt, J. Cardenas, Y. Okawachi, A. Bryant, A. L. Gaeta, and M. Lipson, "Ultra-low-loss on-chip resonators with sub-milliwatt parametric oscillation threshold," *Optica* **4**, 619-624 (2017).